

RESEARCH ARTICLE

Cerebral blood perfusion deficits using dynamic susceptibility contrast MRI with gadolinium chelates in rats with post-ischemic reperfusion without significant dynamic contrast-enhanced MRI-derived vessel permeabilities: A cautionary note

Seokha Jin, MungSoo Kang, HyungJoon Cho*

Department of Biomedical Engineering, Ulsan National Institute of Science and Technology, Ulsan, South Korea

* hjcho@unist.ac.kr



OPEN ACCESS

Citation: Jin S, Kang M, Cho H (2018) Cerebral blood perfusion deficits using dynamic susceptibility contrast MRI with gadolinium chelates in rats with post-ischemic reperfusion without significant dynamic contrast-enhanced MRI-derived vessel permeabilities: A cautionary note. PLoS ONE 13(7): e0201076. <https://doi.org/10.1371/journal.pone.0201076>

Editor: Quan Jiang, Henry Ford Health System, UNITED STATES

Received: May 20, 2018

Accepted: July 6, 2018

Published: July 25, 2018

Copyright: © 2018 Jin et al. This is an open access article distributed under the terms of the [Creative Commons Attribution License](https://creativecommons.org/licenses/by/4.0/), which permits unrestricted use, distribution, and reproduction in any medium, provided the original author and source are credited.

Data Availability Statement: All relevant data are within the paper and its Supporting Information file.

Funding: This research was supported by a grant of the Korea Health Technology R&D Project through the Korea Health Industry Development Institute (KHIDI), funded by the Ministry of Health & Welfare, Republic of Korea (grant number: HI18C0713 to SJ). This work was also supported

Abstract

In this study, we quantified perfusion deficits using dynamic susceptibility contrast magnetic resonance imaging (DSC-MRI) with an extravasating contrast agent (CA). We also investigated the efficacy of leakage compensation from CA pre-load in brains from post-ischemic rat models without significant dynamic contrast-enhanced MRI (DCE-MRI)-derived vessel wall permeability. DSC measurements were obtained using fast (0.3 s) echo-planar imaging in both normal rats and rats with transient middle carotid artery occlusion (MCAO) (1-h MCAO, 24-h reperfusion) after successive administrations of gadoterate meglumine (Dotarem) and intravascular superparamagnetic iron oxide nanoparticles (SPION). The relative cerebral blood volume (CBV) and cerebral blood flow (CBF) values acquired using Dotarem were significantly underestimated (~20%) when compared to those acquired using SPION in ipsilesional post-ischemic brain regions. A slight overestimation of relative mean transit time was observed. Areas with underestimated CBV and CBF values from the corresponding error maps encompassed the area of infarcted tissue (apparent diffusion coefficient < 500 $\mu\text{m}^2/\text{s}$) and mostly coincided with the area wherein conspicuous longitudinal relaxation time differences were observed pre- vs. post-injection of Dotarem. The DSC measurements with significant pre-load (0.3 $\text{mmol}\cdot\text{kg}^{-1}$) of Dotarem displayed minimal perfusion deficits when compared to those determined using the reference intravascular SPION.

Introduction

Post-ischemic reperfusion measurements in small animal models provide useful information for the optimization of intervention therapies and the evaluation of prognostic assessments [1,2]. As brain perfusion provides important information regarding the functional status of

by the 2018 Research Fund (grant number: 1.180063.01 to HC) of the Ulsan National Institute of Science and Technology (UNIST). The funders had no role in study design, data collection and analysis, decision to publish, or preparation of the manuscript.

Competing interests: The authors have declared that no competing interests exist.

stroke lesions, several investigations have been carried out to develop accurate magnetic resonance (MR) measurements and delineation strategies for post-ischemic hypo- and hyper-perfused lesions [3,4]. Dynamic susceptibility contrast MR imaging (DSC-MRI) provides highly sensitive perfusion information and can be used to estimate the exogenous tracer concentration. Thus, it can also be used to extract information regarding cerebral perfusion, including cerebral blood flow (CBF), cerebral blood volume (CBV), and mean transit time (MTT), based on drug tracer models [5–7]. Typically, such pharmacokinetic models assume that the bolus-injected contrast agent (CA) does not extravasate and that the underlying blood vessels are randomly oriented. These are reasonable assumptions for a normal brain with an intact blood-brain barrier (BBB) when using gadoterate meglumine (Dotarem, Guerbet). However, when the BBB is disrupted (e.g., due to the presence of tumors or stroke), Dotarem, which is a member of the most commonly used family of MRI CAs, leaks through vessel walls. Consequently, in the presence of a damaged BBB, the DSC-MRI signal is significantly different from that calculated based on the no-leak assumption. Several studies have reported apparent DSC-MRI signal underestimations and correction methods for extravasating CAs used to image tumors with leaky vessels [8–13].

In studies of brains with early (<24 h) post-ischemic reperfusion and relatively small BBB leakage (insignificant K^{trans} obtained based on DCE-MRI [14]), the resulting DSC-MRI perfusion deficits are sometimes overlooked. In addition, the efficacy of leakage compensation using CA pre-load has not been directly quantified in a post-ischemic animal model. Systematic underestimations of cerebral perfusion parameters derived using DSC-MRI are problematic, especially for longitudinal animal studies, even if they are much smaller than those observed in cases of leaky tumors. This is because the DSC-MRI findings will result in ambiguity in the CBF and CBV threshold criteria used to distinguish the normal and hyper-perfused areas of the lesion. A previous study compared leaky vessel-derived CBF values obtained using DSC-MRI to those obtained using another MRI modality, namely, arterial spin labeling, in a stroke model [15]. However, these values were not compared to those obtained using an intravascular CA.

Accurate monitoring of first-pass (0–4 s in rat, as shown in S1 Fig) DSC time curves requires fast acquisition methods, such as echo-planar imaging (EPI), for application in animal models. This renders DSC-MRI signals much more sensitive to T_1 and susceptibility changes due to CA leakage in animal model studies. Post-ischemic hyper-perfusion (~1 day) was frequently reported in the 1-hour middle cerebral artery occlusion (MCAO) animal model, which potentially has compromised BBB integrity in post-ischemic brain regions [3]. Therefore, a systematic comparison between dual DSC-MRI methods using extravasating and intravascular CAs in this model may be used to quantify and localize the perfusion errors and efficacy of CA pre-load in brains subjected to post-ischemic reperfusion.

In this study, an additional intravascular SPION measurement served as a reference to eliminate the confounding factor of vessel wall permeability following fast (repetition time [TR] = 0.3 s) DSC-MRI acquisition with EPI using Dotarem [13]. The DSC-MRI time curves obtained using either Dotarem or SPION were then directly compared for both normal rats and rats subjected to transient (1-hour) middle carotid artery occlusion (tMCAO) surgery following 1-day reperfusion. The cerebral blood perfusion underestimation errors were then quantified. The measured perfusion underestimation errors for both CAs and the apparent diffusion coefficient (ADC) values were used to segment the ipsi-stroke hemisphere. Cerebral perfusion errors, ADCs, and relative CBV values were compared among the infarct, peri-infarct, and normal zones. The efficacy of leakage compensation due to CA pre-load in brains from post-ischemic rat models was then studied using fast DSC-MRI acquisitions.

Methods

Animal preparation

The experiments were approved by the Institutional Animal Care and Use Committee of Ulsan National University of Science and Technology. Female Sprague-Dawley rats (SD; weight: 150–250 g) were obtained from Orient Bio (Gyeonggi, Republic of Korea). The SD rats were anesthetized with isoflurane during the MRI scan. To compare the two different DSC-MRI derived perfusion maps, rats in the normal ($n = 3$) and stroke ($n = 6$) groups were injected twice with the different CAs (Dotarem and SPION), as shown in [S2 Fig](#). Two Dotarem injections were also performed in normal rats ($n = 3$). For both leakage compensation and vessel wall permeability estimations, DCE-MRI acquisition was performed before the two DSC-MRI acquisitions in the additional stroke group ($n = 3$). Rats in the stroke group were subjected to 1-h intraluminal monofilament (0.35 mm diameter filament, Doccol Corporation, USA) MCAO followed by 1-day reperfusion.

Magnetic resonance imaging

All studies were performed using a 7-T MR scanner (Bruker, Germany) with a 40-mm volume coil and a surface coil. Dotarem and SPION were injected to evaluate the area under the curve (AUC) values of the DSC signals for the extravasating and intravascular CAs, respectively. AUC values for successive Dotarem-Dotarem injections were obtained in the control experiments using normal rats ($n = 3$). Corresponding values for successive Dotarem-SPION injections were also obtained ($n = 3$). For the tMCAO model, AUC values for successive Dotarem-SPION injections were obtained in rats subjected to stroke and reperfusion ($n = 6$). To identify regions of damaged BBB in the rats subjected to stroke, we obtained pre- and post-injection T_1 maps. ADC maps and T_2 -weighted images were also obtained for rats subjected to stroke. All of the MRI procedures are detailed in [S2 Fig](#). For both leakage compensation and vessel wall permeability estimations, the DCE-MRI acquisitions were performed before the two DSC-MRI acquisitions (Dotarem-SPION injections) in the additional stroke group ($n = 3$).

The DSC-MRI perfusion maps were acquired using a gradient-echo EPI sequence with the following pulse sequence parameters: TR = 300 ms, effective echo time (TE) = 17 ms, field of view (FOV) = $30 \times 30 \text{ mm}^2$, matrix size = 96×96 , number of slices = 3, number of averages (NA) = 1, slice gap = 0.2 mm, slice thickness = 1 mm, bandwidth = $3.5 \times 10^5 \text{ Hz}$, number of segments = 1, flip angle = 35° , and temporal resolution = 0.3 s. The Dotarem and SPION injection doses were $0.3 \text{ mmol} \cdot \text{kg}^{-1}$ (130 μl) and $0.075 \text{ mmol} \cdot \text{kg}^{-1}$ (75 μl), respectively.

The T_1 maps were obtained using rapid acquisition with relaxation enhancement (RARE) with variable TR (RAREVTR [16]) with the following parameters: TR = 80, 150, 200, 400, 800, 1200, 1600, 2000, 2500, 3000, and 4500 ms; RARE factor = 4; effective TE = 4.58 ms; NA = 1; FOV = $30 \times 30 \text{ mm}^2$; matrix size = 96×96 ; number of slices = 3; slice gap = 0.2 mm; and slice thickness = 1 mm.

The ADC maps were acquired using diffusion-weighted EPI with the following parameters: TR = 5000 ms; number of segments = 4; effective TE = 20 ms; b-values = 200, 400, 600, and $1000 \text{ s} \cdot \text{mm}^{-2}$; NA = 1; FOV = $30 \times 30 \text{ mm}^2$; matrix size = 96×96 ; number of slices = 3; slice gap = 0.2 mm; and slice thickness = 1 mm. Three ADC maps along the x , y , and z directions were averaged to obtain trace ADC values.

The T_2 -weighted images were obtained using RARE [17] with the following parameters: TR = 5000 ms, RARE factor = 4, effective TE = 30 ms, NA = 2, FOV = $30 \times 30 \text{ mm}^2$, matrix size = 256×256 , number of slices = 20, slice gap = 0 mm, and slice thickness = 0.5 mm.

DCE-MRI data were acquired using fast low angle shot [18] with the following parameters: TR = 35 ms, TE = 1.9 ms, NA = 1, FOV = 30 × 30 mm², matrix size = 96 × 96, number of slices = 3, slice thickness = 1 mm, number of repetitions = 180, temporal resolution = 3.36 s, and flip angle = 30°. The Dotarem injection dose for DCE-MRI was 0.1 mmol·kg⁻¹. The Dotarem injection was followed by a 0.1–0.2 mmol·kg⁻¹ flush (after 15 min) after the acquisition in studies of leakage compensation with CA pre-load for the subsequent fast DSC-MRI [13].

Data analysis

For the *in vivo* study, two relative CBV (rCBV) maps for the first and second CA administrations were estimated from the AUC measurements from 0 to 4 s. The equation $\Delta R_2^*(t)$ ($= -\frac{1}{TE} \ln\left(\frac{S_{post}(t)}{S_{pre}}\right)$) should capture the first-passage of CA, as shown in S1 Fig. Both rCBV maps acquired before the normalization process are shown in S3 Fig. Because the two AUC maps contained relative values, the AUC map of the first administration (Dotarem) was normalized to that of the second administration (SPION) for the region with an intact BBB. For the normalization, the intact-BBB region was drawn manually on the right (normal group) or contralateral (stroke group) hemisphere. As shown in S3 Fig, scatterplots and linear fittings were performed for both AUC_{Dotarem} and AUC_{SPION} values for the intact-BBB region. The AUC_{Dotarem} map obtained after the first injection was then divided based on the slope of the regressed line for the intact-BBB region. The corresponding normalized AUC_{Dotarem} map (nAUC_{Dotarem}) is referred to as rCBV_{Dotarem}. Similarly, the AUC_{SPION} map is referred to as rCBV_{SPION}. Following the above normalization procedure, the AUC ratio between the first and second injections was always 1 by definition ($y = x$) for intact-BBB regions, as shown in S3 Fig. Consequently, the rCBV_{Dotarem} values for the stroke region can be directly compared to those in the reference rCBV_{SPION}. rCBF_{SPION}, rCBF_{Dotarem}, the relative MTT for SPION (rMTT_{SPION}), and rMTT_{Dotarem} were also calculated. The rCBV_{error} map was computed by dividing the rCBV_{SPION} map by the rCBV_{Dotarem} map. We used a similar procedure to generate the rCBF_{error} and rMTT_{error} maps. For the statistical comparisons, a region of interest (ROI) was defined in the left hemisphere (normal group) or the BBB-disrupted region (stroke group). For the stroke group, the BBB-disrupted region was identified using the T_1 difference map, which illustrates the difference between the T_1 maps obtained before and after the Dotarem injection.

Voxel-wise ADC values ($S = S_0 \times e^{-ADC \times b}$) were estimated for three gradient directions and averaged to obtain the ADC map. Areas of infarction ($ADC < 500 \mu\text{m}^2/\text{s}$), peri-infarction with BBB damage ($ADC > 500 \mu\text{m}^2/\text{s}$, $rCBV_{error} > \text{threshold}$), and normal tissue ($ADC > 500 \mu\text{m}^2/\text{s}$, $rCBV_{error} < \text{threshold}$) were segmented by thresholding each value correspondingly in the ipsi-stroke hemisphere [19]. The threshold value was equal to $(\text{mean}_{rCBV_{error}^{contra.}} + \text{std}_{rCBV_{error}^{contra.}})$, where $\text{mean}_{rCBV_{error}^{contra.}}$ and $\text{std}_{rCBV_{error}^{contra.}}$ were the average value and standard deviation of $rCBV_{error}$ in the intact contralateral brain hemisphere, respectively. Histograms of the ADC, $rCBV_{error}$, and $rCBV_{SPION}$ (V_p) values for the corresponding areas were then generated for use in the characterizations.

For the vessel wall permeability estimation, the DCE-MRI time curves were converted to ΔR_1 values and fitted using the extended Toft model [20] to estimate K^{trans} , V_e , and V_p . Pre- and post-injection T_1 values were also sequentially measured in order to enable longitudinal monitoring of the leakage of Dotarem. The efficacy of leakage compensation using CA preload (0.1 mmol·kg⁻¹ for DCE-MRI followed by a 0.1–0.2 mmol·kg⁻¹ flush) was investigated by comparing the rCBV maps for the subsequent Dotarem- and SPION-derived DSC-MRI data.

Results

Extravasating (Dotarem) and intravascular (SPION) CAs in the 1-h MCAO 1-day reperfusion rat model

To evaluate the extent of extravasation for both Dotarem and SPION injections, T_1 maps were measured before and after the CA injections. As shown in S4 Fig, the T_1 values of the infarction region ($ADC < 500 \mu m^2/s$) were significantly lower than those of the contralateral region (Wilcoxon rank sum test, $p < 0.01$, $p = 0.001$) after the Dotarem injection (0.3 mmol/kg) in the tMCAO model. In contrast, no significant differences were observed between the pre- and post-injection T_1 maps (Wilcoxon rank sum test, $p > 0.05$, $p = 0.229$) after the SPION injection, indicating the absence of significant leakage of SPION at this time point. Note that the large-vessel region of the contralateral hemisphere was avoided when manually drawing the ROI because this region exhibited a shortened T_1 value even though the CA was not extravasated. The same ROI was used to compare the Dotarem and SPION results. Statistical analysis of the differences in T_1 measurements pre- vs. post-SPION injection confirmed that SPION did not extravasate to a noticeable degree in rats subjected to 1-h tMCAO and 1-day reperfusion, as shown in S4 Fig.

Comparisons of DSC-MRI times curves obtained following Dotarem vs. SPION injections

The experimental DSC-MRI-derived $\Delta R_2^*(t)$ curves for rats in the normal and tMCAO groups are shown in Fig 1A and 1C, respectively. The black arrows in the SPION time curves in Fig 1C indicate the apparent second peak due to recirculation [6,21]. This peak was usually unobservable in the Dotarem time curves. After the normalization of $AUC_{Dotarem}$ to AUC_{SPION} , $rCBV_{Dotarem}$ ($nAUC_{Dotarem}$) was significantly smaller than $rCBV_{SPION}$ (AUC_{SPION}) for the

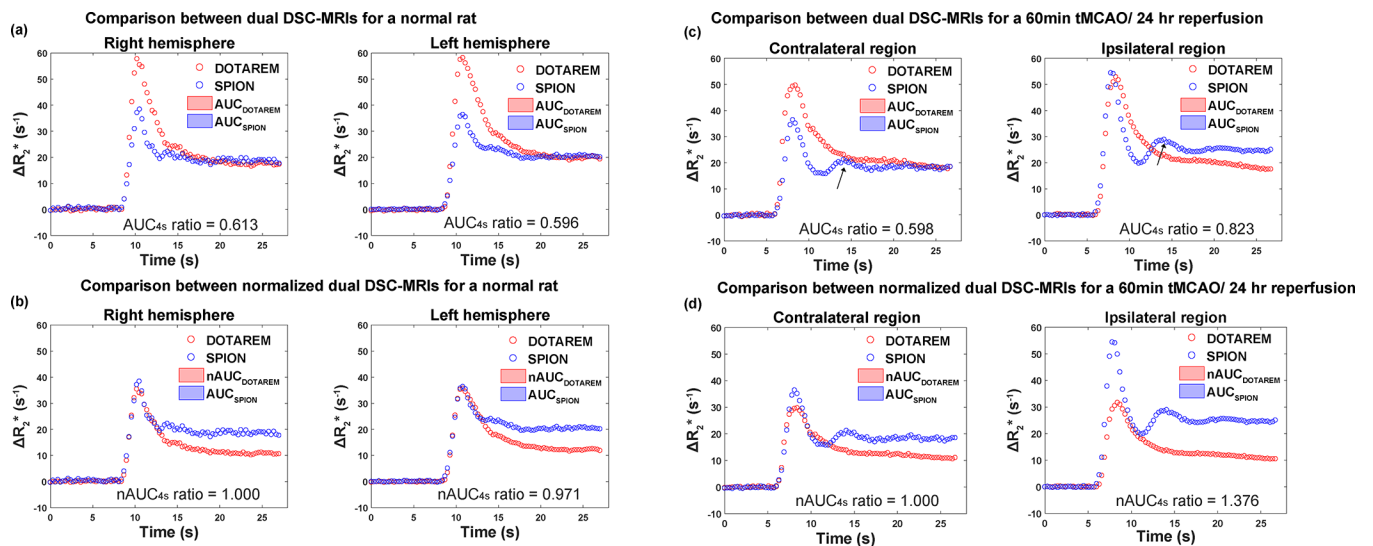


Fig 1. The process of nAUC ratio value estimation. (a) ΔR_2^* curve and AUC of SPION and Dotarem for unnormalized DSC-MRI signal of normal rat. Corresponding AUC ratio values were 0.613 and 0.596 for right and left hemispheres, respectively. (b) ΔR_2^* curve and AUC of SPION and Dotarem for normalized DSC-MRI signals of normal rat. Corresponding nAUC ratio values were 1 and 0.971 for right and left hemispheres, respectively. (c) ΔR_2^* curve and AUC of SPION and Dotarem for unnormalized DSC-MRI signal of tMCAO rat. Corresponding AUC ratio values were 0.598 and 0.823 for contralateral and ipsilateral hemisphere, respectively. (d) ΔR_2^* curve and AUC of SPION and Dotarem for normalized DSC-MRI signal of tMCAO rat. Corresponding nAUC ratio values were 1 and 1.376 for right and left hemispheres, respectively. Black arrows in (c) represent the second peak from recirculation from SPION DSC-MRI times curves.

<https://doi.org/10.1371/journal.pone.0201076.g001>

ipsilesional hemisphere in the tMCAO model (Fig 1D). $rCBV_{error}$ was thus greater than 1 for the BBB-disrupted model. No significant differences in $rCBV_{Dotarem}$ were observed between the two hemispheres in rats in the normal group (Fig 1B). $rCBV_{error}$ was thus close to 1 for rats in the normal group, which did not have blood vessels with BBB disruption. In rats in the normal group, the AUC ratios were 0.613 and 0.596 for the right and left hemispheres, respectively. The corresponding $rCBV_{error}$ values were 1 (by definition) and 0.971 for the right and left hemispheres, respectively. In rats subjected to tMCAO, the AUC ratios were 0.598 and 0.823 for the contralateral and ipsilateral hemispheres, respectively. This indicates post-ischemic hyper-perfusion caused by the SPION injection in the ipsilateral (ischemic) brain hemisphere [1]. The same hyper-perfusion was not observed following the Dotarem injection, presumably due to CBV and CBF underestimations associated with BBB leakage. The corresponding $rCBV_{error}$ values were 1 (by definition) and 1.376 for the right and left hemispheres, respectively. The $rCBV_{error}$ values for the six rats in the stroke group in this study are summarized in Table 1.

Quantified DSC-derived perfusion errors for normal and post-ischemic rat brains

Fig 2 shows the rCBV results for the Dotarem-Dotarem and Dotarem-SPION injections in normal rat brains, respectively. Fig 2A and 2B show the $rCBV_{Dotarem}^{1st}$ (first injection) and $rCBV_{Dotarem}^{2nd}$ (second injection) maps, which are used as controls, respectively. No noticeable differences were observed between the maps. Fig 2C displays the scatterplot of $rCBV_{Dotarem}^{1st}$ values against $rCBV_{Dotarem}^{2nd}$ values in the left hemisphere. Fig 2D and 2E show the $rCBV_{Dotarem}$ (first injection) and $rCBV_{SPION}$ (second injection) maps, respectively. No noticeable difference was observed between these maps, either. Finally, Fig 2F presents the scatterplot of $rCBV_{Dotarem}$ values against $rCBV_{SPION}$ values in the left hemisphere. The absence of significant differences ($rCBV_{error}$ values were close to 1 for rats in the normal group) between $rCBV_{Dotarem}^{1st}$ and $rCBV_{Dotarem}^{2nd}$, and $rCBV_{Dotarem}$ and $rCBV_{SPION}$ confirm the consistency of the rCBV measurements obtained following successive CA injections of Dotarem and SPION (criterion standard) in non-leaking vasculature (normal condition) [22]. Fig 2G summarizes the statistical analysis results for each group. There were no significant differences (Wilcoxon rank sum test, $p > 0.05$, $p = 0.136$).

Fig 3 shows plots of cerebral perfusion measurement errors, such as $rCBV_{error}$, $rCBF_{error}$, and $rMTT_{error}$, for cases of post-ischemic local hypo- and hyper-perfusion. As seen in the ADC maps (Fig 3A2 and 3E2), the decreased ADC values and hyperintense T_2 -weighted images (Fig 3A1 and 3E1) of the left hemisphere indicate the presence of ischemic stroke lesions after tMCAO reperfusion. Fig 3A3 and 3E3 illustrate the differences in the T_1 maps before and after the Dotarem injection. The significant differences in T_1 values in the ipsilateral hemisphere provide a clear indication of Dotarem leakage. No differences in T_1 values were observed following the SPION injections. Fig 3B1 and 3F1 and Fig 3B2 and 3F2, show the $rCBV_{SPION}$ and the $rCBV_{Dotarem}$ maps, respectively, while Fig 3B3 and 3F3 show the resulting $rCBV_{error}$ due to CA extravasation. Fig 3C1 and 3G1, and Fig 3C2 and 3G2, show the $rCBF_{SPION}$ and the $rCBF_{Dotarem}$ maps, respectively, while Fig 3C3 and 3G3 show the resulting $rCBF_{error}$. Fig 3D1 and 3H1 and Fig 3D2 and 3H2, show the $rMTT_{SPION}$ and $rMTT_{Dotarem}$ maps, respectively, while Fig 3D3 and 3H3 show the resulting $rMTT_{error}$. In the case of hypo-perfusion, both $rCBF_{SPION}$ and $rCBF_{Dotarem}$ indicate the presence of post-ischemic ipsilateral hypo-perfusion with respect to the contralateral hemisphere, as indicated by the white arrow in Fig 3C2. In contrast, in the case of hyper-perfusion, $rCBF_{SPION}$ indicates the presence of significant post-ischemic hyper-perfusion, while $rCBF_{Dotarem}$ has non-significant differences with

Table 1. Mean and standard variations of ADC and rCBV error values for infarction, peri-infarction, and normal areas for six rats shown in Figs 4, 5 and 6.

	Rat ₁			Rat ₂			Rat ₃			Rat ₄			Rat ₅			Rat ₆		
	ADC ($\times 10^6 \mu\text{m}^2/\text{s}$)	rCBV (a.u.)	rCBV error (a.u.)	ADC ($\times 10^6 \mu\text{m}^2/\text{s}$)	rCBV error (a.u.)	rCBV (a.u.)	ADC ($\times 10^6 \mu\text{m}^2/\text{s}$)	rCBV error (a.u.)	rCBV (a.u.)	ADC ($\times 10^6 \mu\text{m}^2/\text{s}$)	rCBV error (a.u.)	rCBV (a.u.)	ADC ($\times 10^6 \mu\text{m}^2/\text{s}$)	rCBV error (a.u.)	rCBV (a.u.)	ADC ($\times 10^6 \mu\text{m}^2/\text{s}$)	rCBV error (a.u.)	rCBV (a.u.)
Normal tissue	715 ± 105	1.063 ± 0.088	1.015 ± 0.270	672 ± 85	1.006 ± 0.109	1.153 ± 0.339	698 ± 86	0.991 ± 0.088	1.070 ± 0.364	681 ± 87	1.023 ± 0.081	1.217 ± 0.524	695 ± 79	0.944 ± 0.096	1.147 ± 0.400	725 ± 85	0.890 ± 0.227	1.138 ± 0.589
Peri-infarct	([^]) 645 ± 96	1.321 ± 0.189	1.124 ± 0.365	([^]) 641 ± 77	1.318 ± 0.224	1.388 ± 0.470	674 ± 59	1.274 ± 0.119	1.383 ± 0.468	([^]) 618 ± 75	1.254 ± 0.081	1.197 ± 0.542	([^]) 642 ± 100	1.295 ± 0.183	1.379 ± 0.592	([^]) 672 ± 94	1.481 ± 0.190	1.574 ± 0.593
Infarct	461 ± 21	1.207 ± 0.283	0.927 ± 0.237	-	-	-	-	-	-	418 ± 38	1.219 ± 0.105	1.315 ± 0.444	413 ± 41	1.248 ± 0.143	1.326 ± 0.420	437 ± 29	1.498 ± 0.147	1.354 ± 0.361

* ($p < 0.01$) denotes Wilcoxon rank-sum test results for ADC values between normal and peri-infarct zones.

^ ($p < 0.01$) denotes Wilcoxon rank-sum test results for rCBV values between peri-infarct and infarct zones. a.u. means arbitrary unit.

<https://doi.org/10.1371/journal.pone.0201076.t001>

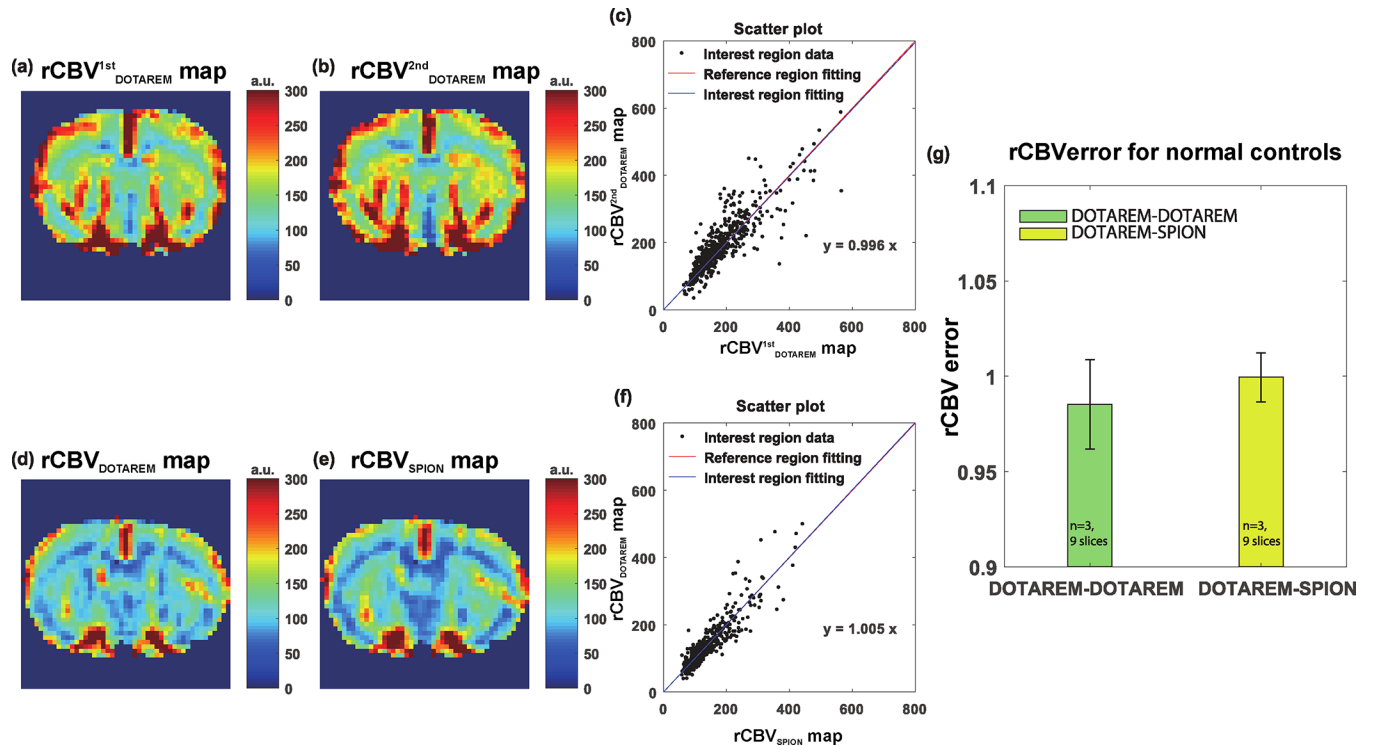


Fig 2. Results of in vivo experiment with normal rats (control experiments). (a) and (b) show the normalized AUC from the first injection ($nAUC_{\text{Dotarem}}$) and the AUC from the second injection (AUC_{Dotarem}), respectively. (c) Scatter plot of $nAUC_{\text{Dotarem}}$ and AUC_{Dotarem} in the left hemisphere (black dots). The red and blue lines are fitted lines to the right- and left-hemisphere scatter plots, respectively. (d) and (e) show the normalized AUC from the first Dotarem injection ($nAUC_{\text{Dotarem}}$) and the AUC from the second SPION injection (AUC_{SPION}), respectively. (f) Scatter plot of $nAUC_{\text{Dotarem}}$ and AUC_{SPION} in the left hemisphere (black dots). The red and blue lines are the corresponding fitted lines to the right- and left-hemisphere scatter plots. (g) Statistical analysis of nAUC ratio. The statistical unit n_{sl} is the number of slices. The green and yellow bar graphs show the nAUC ratio values in the Dotarem-Dotarem and Dotarem-SPION cases, respectively, in normal rats (green bar: 0.990 ± 0.023 [mean \pm standard deviation, $n = 3$, with 9 slices], yellow bar: 1.002 ± 0.017 [$n = 3$ with 9 slices], $p > 0.05$ [$p = 0.136$]). a.u. means arbitrary unit.

<https://doi.org/10.1371/journal.pone.0201076.g002>

respect to the contralateral hemisphere, as indicated by the white arrow in Fig 3G2. These results clearly indicate that the DSC-MRI-derived CBV and CBF values were significantly underestimated when using gadolinium chelates, and in this case, led to errors in the detection of post-ischemic hyper-perfusion. In the ipsi-stroke hemisphere in both cases, the corresponding $rCBV_{\text{error}}$ and $rCBF_{\text{error}}$ were apparent not only in the infarcted zone ($ADC < 500 \mu\text{m}^2/\text{s}$), but also in the peri-infarcted area. The boundaries of the region with significant $rCBV_{\text{error}}$ and $rCBF_{\text{error}}$ values mostly matched those of the corresponding T_1 difference map, indicating the leakage of Dotarem. The BBB leakage-derived errors did not appear to correlate with the V_p ($rCBV_{\text{SPION}}$) values. It was also noted that when compared to the values obtained following the SPION injection, the $rCBV_{\text{Dotarem}}$ and $rCBF_{\text{Dotarem}}$ values were generally underestimated, and the $rMTT_{\text{Dotarem}}$ value was slightly overestimated. Fig 3I shows differences in the slopes of the scatterplots for the three perfusion indices obtained following the use of Dotarem and SPION in the BBB-disrupted region. The ROIs for these scatterplots were obtained from the corresponding T_1 difference maps. Rats in the normal group were used as controls. The perfusion parameters calculated in these rats were compared to those calculated in rats in the stroke group (Fig 3J). The $rCBV_{\text{error}}$ values for lesions in BBB-disrupted regions differed significantly from those obtained in rats in the control group (Wilcoxon rank sum test, $p < 0.01$, $p = 1.98 \times 10^{-7}$). In other words, the $rCBV_{\text{Dotarem}}$ values for lesions in the BBB-disrupted regions were estimated to be significantly lower ($\sim 20\%$) than the corresponding $rCBV_{\text{SPION}}$ values.

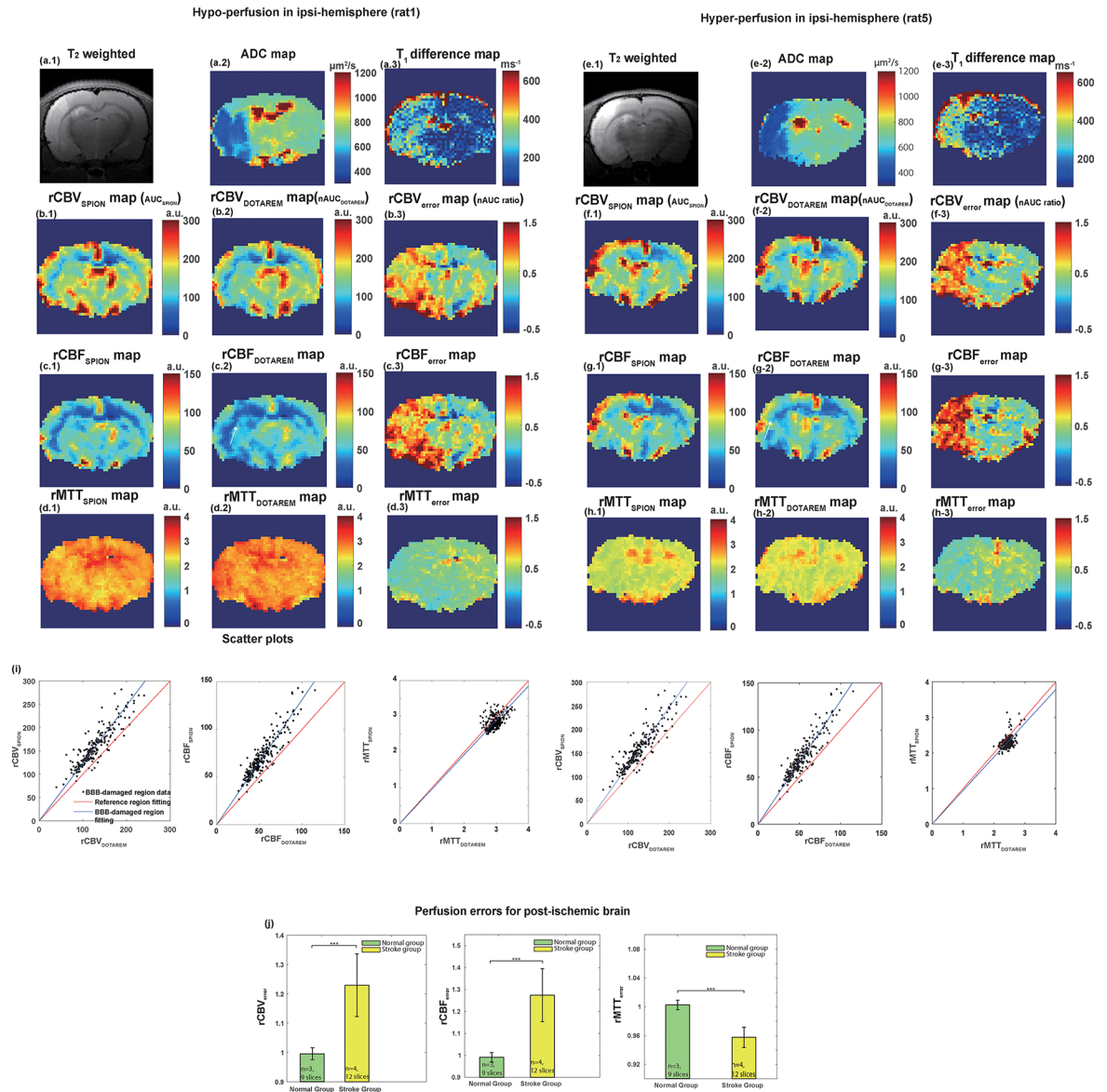


Fig 3. Results of in vivo experiment on two stroke rats with local hypo- and hyper-perfusion. (a.1, e.1) T_2 -weighted images, (a.2, e.2) ADC maps, and (a.3, e.3) T_1 map difference between pre- and post-Dotarem injection. (b.1, f.1) and (b.2, f.2) show the $rCBV_{SPIO}$ (AUC_{SPIO}) and $rCBV_{Dotarem}$ ($nAUC_{Dotarem}$), respectively. (b.3, f.3) show the associated $rCBV_{error}$ ($nAUC_{ratio}$). (c.1, g.1) and (c.2, g.2) show the $rCBF_{SPIO}$ and $rCBF_{Dotarem}$, respectively. (c.3, g.3) show the associated $rCBF_{error}$. (d.1, h.1) and (d.2, h.2) show the $rMTT_{SPIO}$ and $rMTT_{Dotarem}$, respectively. (d.3, h.3) show the associated $rMTT_{error}$. (i) Respective scatter plots of $rCBV_{SPIO}/rCBV_{Dotarem}$, $rCBF_{SPIO}/rCBF_{Dotarem}$, and $rMTT_{SPIO}/rMTT_{Dotarem}$ in the damaged BBB ipsi-lesional hemisphere of stroke (black dots). The red and blue lines are fitted lines for the contralateral hemisphere and the BBB-disrupted lesion, respectively. (j) Respective statistical analysis of corresponding perfusion parameters. The green and yellow bar graphs represent the values from the normal ($n = 3$ with 9 slices) and stroke groups ($n = 4$ with 12 slices), respectively. a.u. means arbitrary unit.

<https://doi.org/10.1371/journal.pone.0201076.g003>

Regional segmentation of post-ischemic brain based on $rCBV_{error}$, ADC, and V_p

In the first column of Fig 4, the infarct ($ADC < 500 \mu m^2/s$) voxels of regions with BBB damage ($rCBV_{error} > threshold$) are shown in red. The infarct ($ADC < 500 \mu m^2/s$) voxels of regions without BBB damage ($rCBV_{error} < threshold$) are shown in yellow, but are scarce. Voxels of

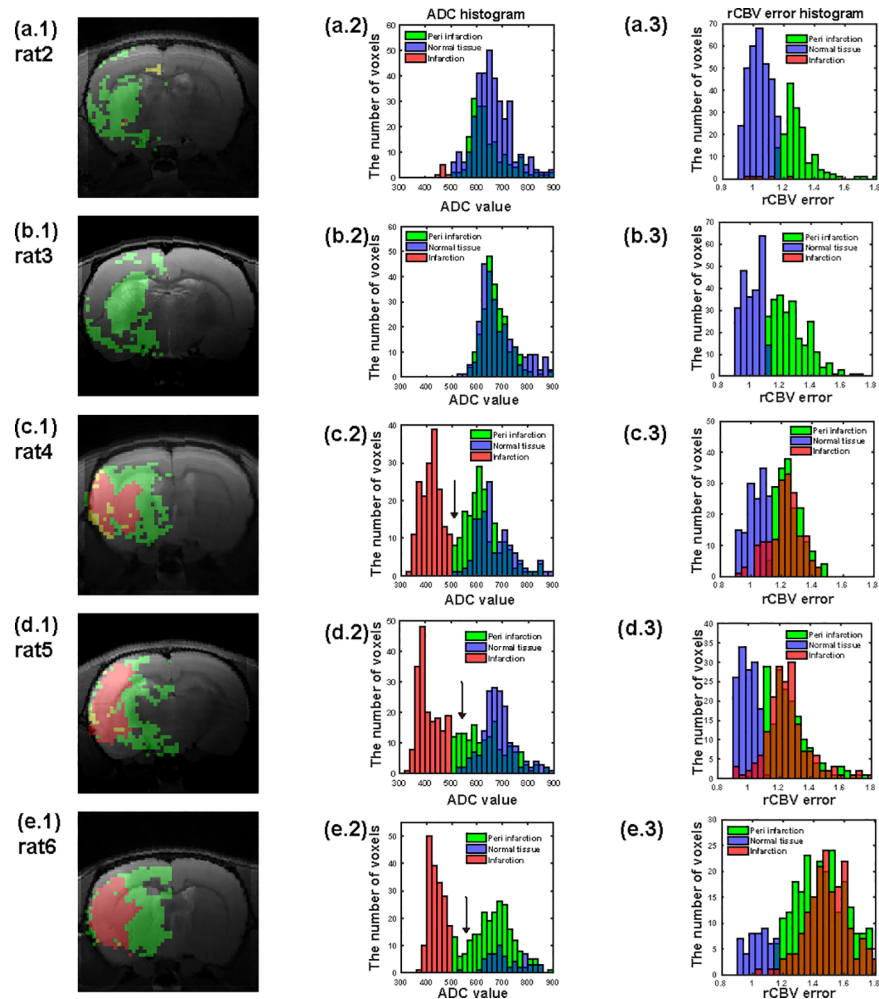


Fig 4. (a.1), (b.1), (c.1), (d.1), (e.1) show infarcted areas with BBB damage ($ADC < 500 \mu m^2/s$ and $rCBV_{error} >$ threshold) in red and peri-infarcted areas with BBB damage ($ADC > 500 \mu m^2/s$ and $rCBV_{error} >$ threshold) in green. Infarcted area without BBB damage ($ADC < 500 \mu m^2/s$ and $rCBV_{error} <$ threshold) is shown in yellow, but scarce. (a.2), (b.2), (c.2), (d.2), (e.2) show histograms of ADC values of corresponding infarcted (red), peri-infarcted with BBB-damage (green), and normal (purple) areas. The normal region satisfies the condition of $ADC > 500 \mu m^2/s$ and $rCBV_{error} <$ threshold. The overlapping ADC values between peri-infarcted (green) and normal (purple) areas are shown in dark blue. (a.3), (b.3), (c.3), (d.3), (e.3) show histograms of $rCBV_{error}$ values corresponding to infarcted (red), peri-infarcted with BBB damage (green), and normal (purple) areas. The overlapping $rCBV_{error}$ values between infarcted (red) and peri-infarcted (green) areas are shown in dark orange.

<https://doi.org/10.1371/journal.pone.0201076.g004>

BBB-damaged regions ($rCBV_{error} >$ threshold) without infarction ($ADC > 500 \mu m^2/s$) are shown in green. The green area may thus represent the peri-infarct area where there is BBB damage. In the second column of Fig 4, the ADC histograms for the infarct ($ADC < 500 \mu m^2/s$), peri-infarct with BBB damage ($ADC > 500 \mu m^2/s$ and $rCBV_{error} >$ threshold), and normal ($ADC > 500 \mu m^2/s$ and $rCBV_{error} <$ threshold) regions are shown in red, green, and purple, respectively. The overlapping ADC values between the peri-infarct (green) and normal (purple) areas are shown in dark blue. For the small lesions shown in the top two rows, the peri-infarct areas had noticeably smaller ADC values than areas of normal tissue. For the larger lesions shown in the bottom three rows, the presence of non-overlapping mid-range ADC values ($500 \mu m^2/s < ADC < 600 \mu m^2/s$) was distinct in the peri-infarct areas when compared to areas of normal tissue (indicated by black arrows on the ADC histograms). In the third column

of Fig 4, $rCBV_{error}$ histograms for the infarct, peri-infarct with BBB damage, and normal regions are shown in red, green, and purple, respectively. The overlapping $rCBV_{error}$ values between the infarct (red) and peri-infarct (green) areas are shown in dark orange. No significant differences were observed in the $rCBV_{error}$ values between the infarct (red) and peri-infarct (green) areas, as most of the red-tagged values overlap with green-tagged areas.

Table 1 summarizes the ADC, $rCBV_{error}$, and $rCBV_{SPION}$ (V_p) values for each region for the six rats subjected to stroke. The ADC values were significantly different for the infarct, peri-infarct, and normal regions. The $rCBV_{error}$ values were significantly different between the infarct (peri-infarct) and normal regions, but no difference was observed between the infarct and peri-infarct regions. The $rCBV_{SPION}$ (V_p) values did not appear to strongly correlate with the applied regional segmentation.

Leakage compensation with CA pre-load

We performed DCE-MRI acquisitions before the DSC-MRI measurements with both Dotarem and SPION in three post-ischemic rats (a T_2 -weighted image and an ADC map for a representative animal are shown in Fig 5A1 and 5A2, respectively). R_1 ($= 1/T_1$) changes are shown for infarcted (green) and normal (blue) regions as a function of post-injection time, where the injection time-points are marked with red lines on the axis in Fig 5A3. No significant T_1 differences (after 10 min) were observed pre- vs. post-injection of Dotarem ($0.1 \text{ mmol}\cdot\text{kg}^{-1}$) in the infarction and normal regions, as shown in Fig 5A4. Similarly, no significant differences in vessel wall permeability (K^{trans}) values obtained using the extended Toft model were observed in the infarction region, as shown in Fig 5A5. After the Dotarem flush ($0.2 \text{ mmol}\cdot\text{kg}^{-1}$ after 15 min), the T_1 values were further reduced in the infarction region, but not in the normal region. This led to a significant difference in T_1 (after 85 min) pre- vs. post-injection, as shown in Fig 5A3.

Perfusion deficits identified using fast DSC-MRI following increasing CA pre-loads are shown in Fig 6. Significant underestimation of $rCBV_{Dotarem}$ with respect to $rCBV_{SPION}$ without

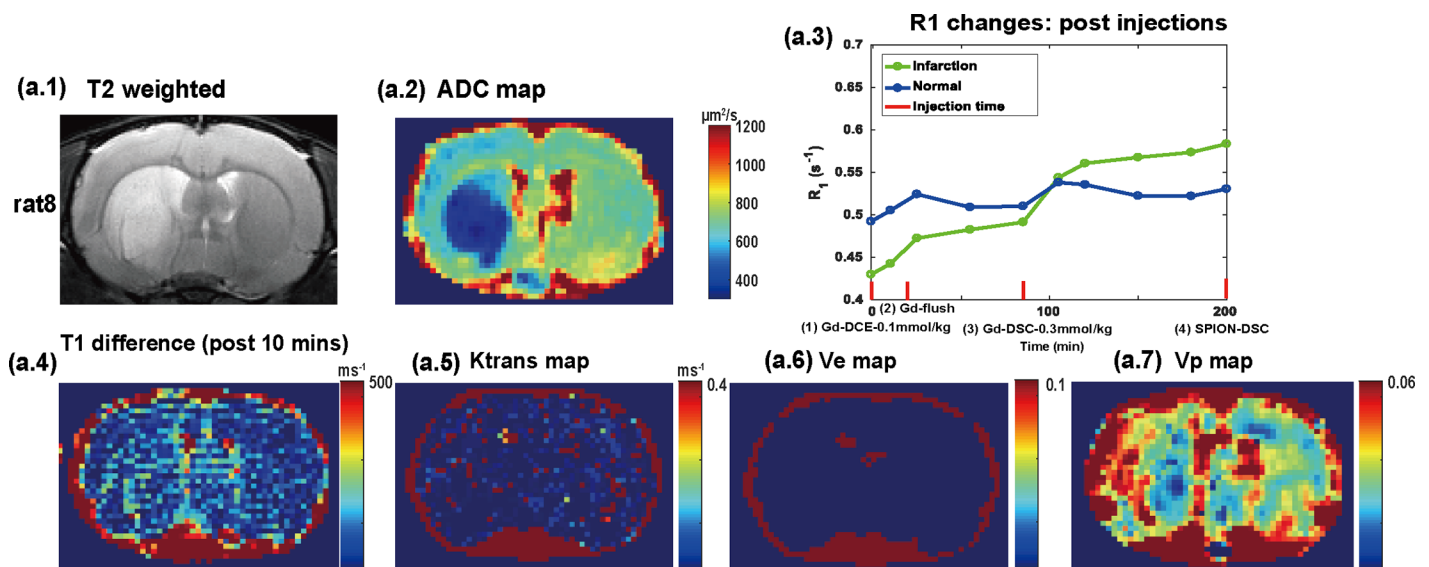


Fig 5. (a.1) T_2 -weighted image. (a.2) ADC map. (a.3) T_1 changes were shown for infarction (green) and normal (blue) region as a function of post-injection time, where injection time-points were marked with red lines. No significant T_1 difference between infarction and normal region were observed from (a.4) T_1 difference map (post-10 mins) after the injection of DOTAREM ($0.1 \text{ mmol}\cdot\text{kg}^{-1}$). (a.5) K^{trans} map. (a.6) V_e map. (a.7) V_p map.

<https://doi.org/10.1371/journal.pone.0201076.g005>

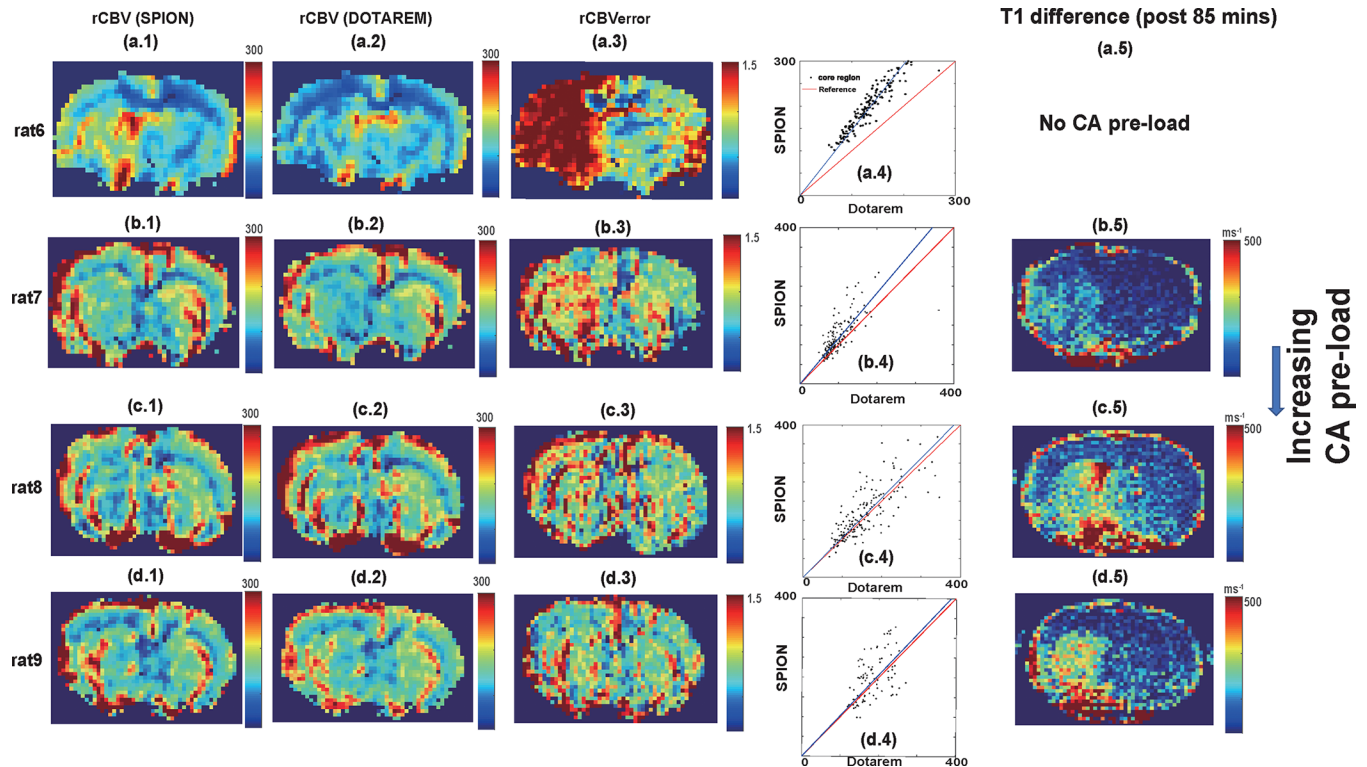


Fig 6. (a.1-d.1) rCBV maps from SPION. (a.2-d.2) rCBV maps from DOTAREM (a.3-d.3) rCBV_{error} map. (a.4-d.4) Scatter plots of rCBV_{SPION}/rCBV_{DOTAREM} values in core region normalized to each normal area. (a.5-d.5) T_1 difference maps (post 85 mins) with increasing CA pre-load. No T_1 difference map was available for no CA pre-load case and not available.

<https://doi.org/10.1371/journal.pone.0201076.g006>

CA pre-load was again apparent, as shown in Fig 6A1, 6A2 and 6A3. However, in the presence of significant CA pre-load (net: 0.3 mmol·kg⁻¹), the SPION and Dotarem rCBV maps were similar and there was minimal rCBV_{error}, as shown in Fig 6C1, 6C2 and 6C3. In another rat with a comparable T_1 difference map and CA pre-load (net: 0.3 mmol·kg⁻¹), we repeatedly observed significantly reduced rCBV_{error}, as shown in Fig 6D1, 6D2 and 6D3. In contrast, in a rat with a less conspicuous T_1 difference map (Fig 6B5), a noticeable underestimation of rCBV_{Dotarem} was still observed, as shown in Fig 6B1, 6B2 and 6B3. Fig 6A4, 6B4, 6C4 and 6D4 compare scatterplots of rCBV values for the core region following Dotarem and SPION injections. Mismatches between the core and normal areas are reduced with increasing CA pre-load, as shown in the enlargement of the T_1 difference map (after 85 min, just before the DSC-MRI acquisition) shown in Fig 6A5, 6B5, 6C5 and 6D5. No significant T_1 changes were observed in the rat without CA pre-load (Fig 6A5, corresponding T_1 differences map is not shown).

Discussion and conclusions

Significant perfusion deficits (rCBV_{error} ~20%) were present in DSC-MRI data obtained using fast (0.3 s) EPI acquisition, even in brains of post-ischemic rats (1-h MCA0, 24-h reperfusion) with insignificant permeability (K^{trans}) values obtained using DCE-MRI with gadolinium chelates administered at the conventional dose of 0.1 mmol·kg⁻¹. Even though it is difficult to separate the effects of T_1 shortening and susceptibility contrast changes from those of leaking CA on DSC-MRI-derived perfusion deficits, fast EPI acquisition will be inevitably affected by T_1 shortening due to the leaky vessels. Nevertheless, in animal model studies with rapid blood

circulation at high magnetic fields, the lengthening of temporal resolution or the increasing of injection dose may not be adequate for the accurate determination of perfusion parameters. As a result, leakage compensation using CA pre-load ($0.3 \text{ mmol}\cdot\text{kg}^{-1}$) may be necessary to avoid perfusion deficits during high temporal resolution DSC-MRI acquisition in animal models of early post-ischemic reperfusion. This is especially true for longitudinal follow-up studies of post-ischemic animal models with varying degrees of vessel wall permeability [14].

It is also worthwhile to note that the DSC signal bias originates from compromised BBB integrity and is likely to be proportional to K^{trans} and inversely proportional to CBV. As a result, the perfusion errors in DSC-MRI data obtained using extravasating vs. intravascular CAs may be particularly sensitive to weakly leaking microvessels with small CBVs. The conspicuous $rCBV_{error}$ in this tMCAO model may thus provide more sensitive diagnostic information than the corresponding ADC and $rCBV_{SPION}$ (V_p) maps. The increased area of the elevated $rCBV_{error}$ values for enlarging infarct regions may articulate the boundaries of the BBB-disrupted areas in the ipsilesional hemisphere in this ischemic reperfusion stroke model. The significantly larger regions with disrupted BBB than the diffusion-reduced (infarction) regions in the tMCAO model indicate peri-infarct BBB-damaged capillaries (Fig 3), which may lead to secondary vascular dysfunction that can limit recovery of viable tissue near an infarcted zone. A few histology-based studies have also confirmed the existence of BBB-damaged capillaries in peri-infarct zones [23,24]. In the peri-infarct BBB-damaged zone determined based on the $rCBV_{error}$ threshold, a significant reduction in the ADC value was apparent between $500 \mu\text{m}^2/\text{s}$ and $600 \mu\text{m}^2/\text{s}$ (Fig 3 and Table 1). The region with slightly decreased ADC values co-localized with the elevated $rCBV_{error}$, and is likely to be a signature of early vasogenic edema, some of which may progress to irreversible infarction.

The potential limitations of this study are as follows. First, direct histological comparison was not possible for the proposed $rCBV_{error}$ values, as independent three-dimensional characterization methods for vessel permeability and flow are scarce. Instead, considering the similar molecular weight of Dotarem (0.56 kDa) to that of traditional Evans blue dye (0.9 kDa), the T_1 difference maps obtained before and after the Dotarem injection ($0.3 \text{ mmol}\cdot\text{kg}^{-1}$) were used to assess BBB leakage in this study. Second, any Dotarem remaining in the tissue may impose a signal bias for the following DSC-MRI performed after the SPION injection. However, as the $\Delta R_2^*(t)$ of the early-phase DSC-MRI was obtained based on the signal differences before vs. after the CA administration rather than from the absolute signals, we assumed that the effects of remaining CA on the second injection were minimal. Future developments in fast T_1 acquisition methods with improved sensitivity [25,26] or the complete separation of T_2^* and T_1 changes in the first-passage signal time courses for the leaky BBB may provide further insights into the biophysical mechanisms underlying multiple CA injections. Third, although the $\Delta R_2^*(t)$ values obtained at 7 T are minimally related to the underlying vessel sizes or shapes [27] and are primarily dependent on CBV and CBF values for randomly oriented vessels, cautious interpretation of T_2^* -based DSC-MRI signals is required due to potential geometric complications and unwanted susceptibility artifacts in post-ischemic brain applications. Future investigation of the effects of unaccounted Dotarem-cell interactions or vessel size effects on dual DSC-MRIs may be pursued in post-ischemic animal models of weak BBB damage.

In summary, we combined two different AUC measurements of sequential DSC-MRIs to characterize cerebral perfusion errors using extravasating (Dotarem) and intravascular (SPION) CAs in the brains of a post-ischemic 60-minute MCAO and 1-day reperfusion rat model. DSC-MRI-derived perfusion indices, such as relative CBF and CBV values obtained using an extravasating CA, were underestimated (~20%). The brain area with a significant $rCBV_{error}$ encompassed the region of infarct tissue and mostly co-localized with the region with T_1 differences pre- vs. post-Dotarem injection. This indicates the presence of a disrupted

BBB in the infarct and peri-infarct regions. The DSC measurements obtained using significant pre-load ($0.3 \text{ mmol}\cdot\text{kg}^{-1}$) of Dotarem had minimal perfusion deficits when compared to those obtained using the reference intravascular SPION.

Supporting information

S1 Fig. (a-1) Dynamic ΔR_2^* curve from SPION in normal rat brain. (a-2) The ROI of the brain location, where the ΔR_2^* curve (a-1) is sampled from. Time intervals of first passage (pre-injection~4s), second passage (4~10s) and steady state (>10s) were defined based on DSC-MR signal with intravascular SPION injection. (b) The ipsilateral (red) and contralateral (green) ROI of the brain locations, where the ΔR_2^* curves of stroke rats were sampled for Fig 1C.

(TIF)

S2 Fig. Experimental schemes of animal preparation and MR scan. (a) Experimental scheme for normal rats. (b) Experimental scheme for stroke group rats. A T_2 -weighted image, ADC map, and T_1 map were additionally obtained for the stroke group rats. The durations for T_2 -weighted image (RARE), ADC map (DW-EPI), T_1 map (RAREVTR), and AUC map (DSC-EPI) acquisitions were 10, 9, 10, and 4 mins, respectively. The duration between the injections for each experiment was 2 hours. The duration for MCAO and following reperfusion was 1 hour and 24 hours, respectively.

(TIF)

S3 Fig. The process of nAUC estimation. (a) and (b) AUC_{DOTAREM} and AUC_{SPION} map from normal rat brain. (c) Scatter plot between AUC_{DOTAREM} and AUC_{SPION} for reference and interest region. (d) $nAUC_{\text{DOTAREM}}$ map, which was divided by the ratio of AUC_{SPION} and AUC_{DOTAREM} ($= 0.573$). (e) Scatter plot between $nAUC_{\text{DOTAREM}}$ and AUC_{SPION} for reference and interest region.

(TIF)

S4 Fig. (a) The T_1 difference before and after the CA injection for 1-hr MCAO and 1-day reperfusion model. The green and yellow bar graphs present the T_1 difference of the ipsilateral infarction ($ADC < 500 \mu\text{m}^2/\text{s}$) and contralateral regions, respectively. The statistical unit n_{sl} is the number of slices. For the DOTAREM case (left), green bar: $252 \pm 94 \text{ ms}$ ($n_{\text{sl}} = 12$), yellow bar: $87 \pm 39 \text{ ms}$ ($n_{\text{sl}} = 12$), and $p < 0.01$ ($p = 0.001$). For the SPION case (right), green bar: $27 \pm 31 \text{ ms}$ ($n_{\text{sl}} = 12$), yellow bar: $47 \pm 26 \text{ ms}$ ($n_{\text{sl}} = 12$), and $p > 0.05$ ($p = 0.229$). (b) The T_1 difference maps for 1-hr MCAO/1-day and 1-hr MCAO/7-day reperfusion models, respectively. Significant leakage of SPION is apparent in 1-hr MCAO/7-day reperfusion model.

(TIF)

S5 Fig. Respective rCBV histograms of normal, peri-infarction, and infarction regions from six stroke rats, which were reported in Table 1.

(TIF)

S6 Fig. The fittings of DCE-MRI time curves, which were used to generate K_{trans} , V_e , and V_p maps shown in Fig 5. Blue and red dots represent time-signal data for normal and infarction regions, respectively.

(TIF)

S7 Fig. The fittings of ADC values, which were used to generate ADC maps shown in Figs 3–5. Blue and red dots represent diffusion data for normal and infarction regions, respectively for six stroke rats.

(TIF)

S8 Fig. The fittings of rCBV values from DSC-MRI, which were used to generate rCBV maps throughout the manuscript.

(TIF)

Acknowledgments

This research was supported by a grant of the Korea Health Technology R&D Project through the Korea Health Industry Development Institute (KHIDI), funded by the Ministry of Health & Welfare, Republic of Korea (grant number: HI18C0713). This work was also supported by the 2018 Research Fund (grant number: 1.180063.01) of the Ulsan National Institute of Science and Technology (UNIST)

Author Contributions

Conceptualization: HyungJoon Cho.

Data curation: Seokha Jin.

Formal analysis: Seokha Jin.

Funding acquisition: HyungJoon Cho.

Methodology: Seokha Jin.

Supervision: HyungJoon Cho.

Validation: Seokha Jin, MungSoo Kang.

Visualization: Seokha Jin.

Writing – original draft: Seokha Jin.

Writing – review & editing: HyungJoon Cho.

References

1. Garcia JH, Experimental ischemic stroke: A review. *Stroke* 1984; 15: 5–14.
2. Hossmann K-A, Animal models of cerebral ischemia: I. Review of literature. *Cerebrovascular Diseases*. 1991; 1: 2–15.
3. Shen Q, Du F, Huang S, Duong TQ. Spatiotemporal characteristics of post-ischemic hyper-perfusion with respect to changes in T1, T2, diffusion, angiography, and blood–brain barrier permeability. *Journal of Cerebral Blood Flow & Metabolism*. 2011; 31(10): 2076–2085.
4. Shen Q, Duong TQ. Magnetic resonance imaging of cerebral blood flow in animal stroke models. *Brain Circulation*. 2016; 2(1): 20. <https://doi.org/10.4103/2394-8108.178544> PMID: 26998527
5. Calamante F, Thomas DL, Pell GS, Wiersma J, Turner R. Measuring cerebral blood flow using magnetic resonance imaging techniques. *Journal of Cerebral Blood Flow & Metabolism*. 1999; 19(7): 701–735.
6. Cha S, Knopp EA, Johnson G, Wetzel SG, Litt AW, Zagzag D. Intracranial Mass Lesions: Dynamic Contrast-enhanced Susceptibility-weighted Echo-planar Perfusion MR Imaging 1. *Radiology*. 2002; 223(1): 11–29. <https://doi.org/10.1148/radiol.2231010594> PMID: 11930044
7. Zierler KL. Theoretical basis of indicator-dilution methods for measuring flow and volume. *Circulation Research*. 1962; 10(3): 393–407.
8. Uematsu H, Maeda M. Double-echo perfusion-weighted MR imaging: basic concepts and application in brain tumors for the assessment of tumor blood-volume and vascular permeability. *European Radiology*. 2006; 16(1): 180–186. <https://doi.org/10.1007/s00330-005-2807-9> PMID: 16402258
9. Boxerman JL, Schmainda KM, Weisskoff RM. Relative cerebral blood-volume maps corrected for contrast agent extravasation significantly correlate with glioma tumor grade, whereas uncorrected maps do not. *American Journal of Neuroradiology*. 2006; 27(4): 859–867. PMID: 16611779

10. Vonken EJPA, van Osch MJP, Bakker CJG, Viergever MA. Simultaneous quantitative cerebral perfusion and Gd-DTPA extravasation measurement with dual-echo dynamic-susceptibility-contrast MRI. *Magnetic Resonance in Medicine*. 2000; 43(6): 820–827. PMID: [10861876](https://pubmed.ncbi.nlm.nih.gov/10861876/)
11. Dósa E, Guillaume DJ, Haluska M, Lacy CA, Hamilton BE, Njus JM, et al. Magnetic resonance imaging of intracranial tumors: intra-patient comparison of gadoteridol and ferumoxytol. *Neuro-oncology*. 2010; 13(2): 251–60. <https://doi.org/10.1093/neuonc/noq172> PMID: [21163809](https://pubmed.ncbi.nlm.nih.gov/21163809/)
12. Quarles CC, Ward BD, Schmainda KM. Improving the reliability of obtaining tumor hemodynamic parameters in the presence of contrast agent extravasation. *Magnetic Resonance in Medicine*. 2005; 53(6): 1307–1316. <https://doi.org/10.1002/mrm.20497> PMID: [15906288](https://pubmed.ncbi.nlm.nih.gov/15906288/)
13. Boxerman JL, Prah DE, Paulson ES, Machan JT, Bedekar D, Schmainda KM. The role of preload and leakage correction in Gadolinium-based cerebral blood volume estimation determined by comparison with MION as a criterion standard. *American Journal of Neuroradiology*, 2012; 33(6): 1081–1087 <https://doi.org/10.3174/ajnr.A2934> PMID: [22322605](https://pubmed.ncbi.nlm.nih.gov/22322605/)
14. Lin CY, Chang C, Cheung WM, Lin MH, Chen JJ, Hsu CY, et al. Dynamic changes in vascular permeability, cerebral blood volume, vascular density, and size after transient focal cerebral ischemia in rats: evaluation with contrast-enhanced magnetic resonance imaging. *Journal of Cerebral Blood Flow & Metabolism*. 2008; 28(8): 1491–501.
15. Tanaka Y, Nagaoka T, Nair G, Ohno K, Duong TQ. Arterial spin labeling and dynamic susceptibility contrast CBF MRI in postischemic hyperperfusion, hypercapnia, and after mannitol injection. *Journal of Cerebral Blood Flow & Metabolism*. 2011; 31(6): 1403–1441.
16. Lee DK, Han SH, Cho H. Optimization of Sparse Phase Encodings for Variable-Repetition-Delay Turbo-Spin Echo (TSE) T1 Measurements for preclinical applications. *Journal of Magnetic Resonance*, 2017; 274: 57–64. <https://doi.org/10.1016/j.jmr.2016.11.004> PMID: [27886558](https://pubmed.ncbi.nlm.nih.gov/27886558/)
17. Hennig J, Nauerth A, Friedburg H. RARE imaging: a fast imaging method for clinical MR, 1986. *Magnetic Resonance in Medicine*, 1986; 3: 823–833. PMID: [3821461](https://pubmed.ncbi.nlm.nih.gov/3821461/)
18. Heisen M, Fan X, Buurman J, van Riel NA, Karczmar GS, ter Haar Romeny BM. The influence of temporal resolution in determining pharmacokinetic parameters from DCE-MRI data. *Magnetic Resonance in Medicine*, 2010; 63(3): 811–816 <https://doi.org/10.1002/mrm.22171> PMID: [20187187](https://pubmed.ncbi.nlm.nih.gov/20187187/)
19. Gill R, Sibson NR, Hatfield RH, Burdett NG, Carpenter TA, Hall LD, et al. A comparison of the early development of ischemic damage following permanent middle cerebral artery occlusion in rats as assessed using magnetic resonance imaging and histology. *Journal of Cerebral Blood Flow & Metabolism*, 1995; 15(1): 1–11.
20. Roberts C, Issa B, Stone A, Jackson A, Waterton JC, Parker GJ. Comparative study into the robustness of compartmental modeling and model-free analysis in DCE-MRI studies. *Journal of Magnetic Resonance Imaging*, 2006; 23(4): 554–563. <https://doi.org/10.1002/jmri.20529> PMID: [16506143](https://pubmed.ncbi.nlm.nih.gov/16506143/)
21. Keston P, Murray A, Jackson A. Cerebral perfusion imaging using contrast-enhanced MRI. *Clinical Radiology*. 2003; 58(7): 505–13. PMID: [12834633](https://pubmed.ncbi.nlm.nih.gov/12834633/)
22. Simonsen CZ, Østergaard L, Vestergaard-Poulsen P, Røhl L, Bjørnerud A, Gyldensted C. CBF and CBV measurements by USPIO bolus tracking: reproducibility and comparison with Gd-based values. *Journal of Magnetic Resonance Imaging*. 1999; 9(2): 342–347. PMID: [10077035](https://pubmed.ncbi.nlm.nih.gov/10077035/)
23. Nahirney PC, Reeson P, Brown CE. Ultrastructural analysis of blood–brain barrier breakdown in the peri-infarct zone in young adult and aged mice. *Journal of Cerebral Blood Flow & Metabolism*. 2016; 36(2): 413–425.
24. Reeson P, Tennant KA, Gerrow K, Wang J, Weiser Novak S, Thompson K, et al. Delayed Inhibition of VEGF Signaling after Stroke Attenuates Blood–Brain Barrier Breakdown and Improves Functional Recovery in a Comorbidity-Dependent Manner. *The Journal of Neuroscience*. 2015; 35(13): 5128–5143. <https://doi.org/10.1523/JNEUROSCI.2810-14.2015> PMID: [25834040](https://pubmed.ncbi.nlm.nih.gov/25834040/)
25. Bauman G, Johnson KM, Bell LC, Velikina JV, Samsonov AA, Nagle SK, et al. Three-dimensional pulmonary perfusion MRI with radial ultrashort echo time and spatial–temporal constrained reconstruction. *Magnetic Resonance in Medicine*. 2015; 73(2): 555–64. <https://doi.org/10.1002/mrm.25158> PMID: [24604452](https://pubmed.ncbi.nlm.nih.gov/24604452/)
26. Johnson KM, Fain SB, Schiebler ML, Nagle S. Optimized 3D ultrashort echo time pulmonary MRI. *Magnetic Resonance in Medicine*. 2013; 70(5): 1241–1250. <https://doi.org/10.1002/mrm.24570> PMID: [23213020](https://pubmed.ncbi.nlm.nih.gov/23213020/)
27. Han SH, Cho JH, Jung HS, Suh JY, Kim JK, Kim YR, et al. Robust MR assessment of cerebral blood volume and mean vessel size using SPION-enhanced ultrashort echo acquisition. *NeuroImage*. 2015; 112: 382–9. <https://doi.org/10.1016/j.neuroimage.2015.03.042> PMID: [25818683](https://pubmed.ncbi.nlm.nih.gov/25818683/)